NASA Contractor Report 185255
AIAA-90-1901

Computational Analysis of the Flowfield of a Two-Dimensional Ejector Nozzle

Y.H. Choi and W.Y. Soh

Sverdrup Technology, Inc.
Lewis Research Center Group
Brook Park, Ohio

June 1990

NASA

National Aeronautics and
Space Administration

COMPUTATIONAL ANALYSIS OF THE FLOWFIELD OF

A TWO-DIMENSIONAL EJECTOR NOZZLE

Y.H. Choi* and W.Y. Soh*
Sverdrup Technology, Inc.
Lewis Research Center Group
Brook Park, Ohio 44142

Abstract

A time-iterative full Navier-Stokes code, PARC, is used to analyze the flowfield of a two-dimensional ejector nozzle system. A parametric study was performed for two controlling parameters, duct to nozzle area ratio and nozzle pressure ratio. Results show that there is an optimum area ratio for the efficient pumping of secondary flow. At high area ratios, a freestream flow passes directly through the mixing duct without giving adequate pumping. At low area ratios, the jet boundary blocks the incoming flow. The nozzle pressure ratio variation shows that the pumping rate increases as the pressure ratio increases, provided there is no interaction between the shroud wall and the shock cell structure.

Introduction

A steady increase in market needs for trans-Pacific aircraft operation renewed national interest in developing a high-speed civil transport (HSCT). Two of the main environmental concerns are airport community noise and engine emission (ozone depletion). This study is related to the community noise. The acoustic challenge to designing HSCT engines is to reduce noise to FAR 36 stage III noise levels while maintaining the economic viability of the aircraft. To meet these requirements and still provide a high level of performance, the development of a low-noise exhaust nozzle design is essential. To date, various noise suppression concepts have been investigated but none have reduced the noise to the FAR 36 stage III requirement in an efficient manner. Progress and development of these technologies are well reviewed in Ref. 1. However, one of the more current, promising technologies is the mixer-ejector concept developed by W. Presz et al.[2-4] The mixer-ejector concept introduces an array of large-scale, low-intensity streamwise vortices into the downstream mixing duct. These vortices enhance mixing through a convective stirring process. This process results in increased pumping performance with more completely mixed flows exiting the ejector shroud, which consequently reduces jet exhaust noise. Various experimental studies are presently being performed by the NASA Lewis Research Center and others to verify this concept and to make it practical for application to HSCT.

Numerous degrees of freedom as well as complexity in the experiment, however, make it difficult to test every possible set of combinations. An analytical or computational approach is necessary to aid the understanding of experimental results and to provide some guidelines for the ongoing experiment. In the present study as a preliminary step to analyzing the flowfield inside the mixer-ejector nozzle, the simplified two-dimensional ejector tested at NASA

---

*Members AIAA.

Lewis is considered first. A schematic of this two-dimensional ejector nozzle is shown in Fig. 1. The ejector is composed of three major components - primary nozzle, secondary inlet, and mixing duct. The secondary flow is drawn from the freestream. The inlet has an elliptical bellmouth to direct the secondary airflow smoothly into the mixing duct. This mixing duct has a diffuser section which lowers the mixing duct pressure to enhance the ejector pumping rate. The diffuser wall angle for the present case is 4°. The mixing duct area can be varied by moving the shroud vertically.

The flow feature in the ejector nozzle system is complicated by the strong inviscid/viscous interaction, freestream entrainment, shock cell structure, and the coexistence of supersonic and subsonic regions. Until now, most of the analytical studies for ejector nozzle systems were based on Von Karman's control volume approach.[5,6] It is necessary, however, to use the complete Navier-Stokes equations to capture the previously mentioned complex phenomena properly. Recently, Deese and Agarwal[7] presented numerical solutions of Navier-Stokes equations for ejector flowfields using a Runge-Kutta time stepping method; their results were for the subsonic flow regime. In the present study, a time-iterative full Navier-Stokes equation solver (PARC code) is used to investigate the ejector flowfields for mainly underexpanded flows.

Features of the ejector flow depend on several parameters - e.g., geometry of the mixing duct, duct to nozzle area ratio, duct length to width ratio, primary nozzle location with respect to the inlet of mixing duct, primary jet pressure, and Reynolds number, etc. In this study, the effects of the two controlling parameters duct to nozzle area ratio (AR) and nozzle pressure ratio (NPR) on the ejector flowfield were investigated. Computational results are compared with experimental results to validate the code.

Governing Equations

The flow through the ejector nozzle can be described by the Navier-Stokes equations. The nondimensional form of the Navier-Stokes equations can be written in the strong conservation-law form and in the generalized coordinate system as follows:

$$\frac{\partial Q}{\partial t} + \frac{\partial E}{\partial \xi} + \frac{\partial F}{\partial \eta} = \frac{1}{Re}\left(\frac{\partial V_\xi}{\partial \xi} + \frac{\partial V_\eta}{\partial \eta}\right) \tag{1}$$

where the primary dependent vector Q is given by

$$Q = \frac{1}{J}\begin{pmatrix} \rho \\ \rho u \\ \rho v \\ e \end{pmatrix} \tag{2}$$

The vectors E and F represent inviscid flux vectors:

$$E = \frac{1}{J}\begin{pmatrix} \rho U \\ \rho u U + \xi_x p \\ \rho v U + \xi_y p \\ (e + p)U \end{pmatrix} \qquad F = \frac{1}{J}\begin{pmatrix} \rho V \\ \rho u V + \eta_x p \\ \rho v V + \eta_y p \\ (e + p)V \end{pmatrix} \tag{3}$$

In these expressions, x and y are the Cartesian coordinates, and ξ and η are the transformed coordinates. The quantity J is the Jacobian of the transformation defined as $\partial(\xi,\eta)/\partial(x,y)$. The variables ρ and p denote density and static pressure, u and v are velocity components in Cartesian coordinates, and e is the total energy per volume defined to be $\rho[i + (u^2 + v^2)/2]$, where i is the specific internal energy. The contravariant velocities U and V are defined as

$$U = \xi_x u + \xi_y v \qquad V = \eta_x u + \eta_y v \tag{4}$$

On the right side of Eq. (1) the vectors V_ξ and V_η represent viscous flux vectors composed of linear combinations of V_x and V_y which are the Cartesian components of the viscous flux vectors:

$$V_\xi = \frac{1}{J}\left(\xi_x V_x + \xi_y V_y\right) \qquad V_\eta = \frac{1}{J}\left(\eta_x V_x + \eta_y V_y\right) \tag{5}$$

The Cartesian viscous vectors V_x and V_y are

$$V_x = \begin{pmatrix} 0 \\ \tau_{xx} \\ \tau_{xy} \\ u\tau_{xx} + v\tau_{xy} - \dfrac{k}{(\gamma - 1)Pr}\dfrac{\partial T}{\partial x} \end{pmatrix} \qquad V_y = \begin{pmatrix} 0 \\ \tau_{xy} \\ \tau_{yy} \\ u\tau_{xy} + v\tau_{yy} - \dfrac{k}{(\gamma - 1)Pr}\dfrac{\partial T}{\partial y} \end{pmatrix} \tag{6}$$

where the components of the shear stress tensor are given by

$$\left.\begin{aligned} \tau_{xx} &= (\lambda + 2\mu)\,\frac{\partial u}{\partial x} + \lambda\,\frac{\partial v}{\partial y} \\[2mm] \tau_{yy} &= (\lambda + 2\mu)\,\frac{\partial v}{\partial y} + \lambda\,\frac{\partial u}{\partial x} \\[2mm] \tau_{xy} &= \mu\left(\frac{\partial u}{\partial y} + \frac{\partial v}{\partial x}\right) \end{aligned}\right\} \tag{7}$$

Here μ is the viscosity, k is the thermal conductivity, and λ is the second coefficient of viscosity. The Re and Pr are the Reynolds number and Prandtl number, respectively. For the present study, the property μ is evaluated by the Sutherland formula as

$$\frac{\mu}{\mu_0} = \left(\frac{T}{T_0}\right)^{3/2}\frac{T_0 + T_s}{T + T_s} \tag{8}$$

3

where T_s is the Sutherland temperature constant. The Navier-Stokes equations are augmented by the equation of state taken here as that of a perfect gas. Thus, the total energy is defined by

$$e = \frac{p}{\gamma - 1} + \rho\left(\frac{u^2 + v^2}{2}\right) \tag{9}$$

where γ is the ratio of specific heats.

In the turbulence calculations, the algebraic turbulence model based on the Thomas formulation of the Baldwin and Lomax model[8,9] is employed for eddy viscosity.

Numerical Procedure

The numerical solution of the Navier-Stokes equations is obtained by the PARC computer code, which is a variant of the ARC code developed by Pulliam et al.[10] The detailed development and some of the recent work related to the PARC code can be found in Ref. 11. In general, the program uses an Euler implicit discretization in time along with central differencing in space for both the inviscid and viscous terms. An efficient solution of the resulting matrix can be obtained by using the approximate factorization based on the Douglas-Gunn procedure[12] with diagonalization of the inviscid terms. In addition, Jameson's type of artificial dissipation[13] is added and treated implicitly for monotonicity and stability. This procedure results in the scalar pentadiagonal matrix which can be inverted in an efficient manner. All equations are solved simultaneously at each time step until convergence to a steady state is reached.

Boundary Conditions

The flow domain of interest is shown in Fig. 1. In the present study, we compute only half of this domain since the flowfield is symmetric. Boundary conditions are specified at the upstream and downstream ends, at the far field, and on all walls. At the upstream boundary stagnation pressure, the stagnation temperature and flow angle (v/u) of the incoming stream are specified. These three boundary conditions are supplemented by extrapolating the left running Riemann invariant. The flowfield at the downstream end is mixed subsonic/supersonic. For the supersonic flow region, since no physical boundary condition is needed, all flow variables are extrapolated. For the subsonic flow region, back pressure is specified for a given freestream Mach number. The no slip condition and thermally adiabatic conditions are imposed on all walls. This condition is again augmented by the normal momentum equation. At the nozzle exit and at the trailing edge of the shroud, a Kutta condition is imposed to ensure the continuity of pressure on both sides of the wall:

$$\left.\frac{\partial p}{\partial n}\right|_{lower} = \left.\frac{\partial p}{\partial n}\right|_{upper}, \qquad p_{lower} = p_{upper}$$

The far-field boundary condition for the present case uses normal velocity $v = 0$, and the remaining flow variables are extrapolated. A symmetry condition is imposed on the plane of symmetry of the computational domain. All the boundary conditions mentioned previously are imposed in an explicit manner.

4

Results and Discussion

To understand the physical flow phenomena in the ejector nozzle system, a parametric study was done for two controlling parameters, mixing duct to nozzle area ratio (AR) and nozzle pressure ratios (NPR). Herein, AR is defined as the ratio of the mixing duct inlet area (As) to the primary nozzle throat area (Ap) (AR = As/Ap, refer to Fig. 1). All calculations are performed on a 171 × 91 grid. The typical grid used for the present calculations is shown in Fig. 2. Grid is clustered near all walls (the first grid line is located at a y^+ of approximately 10.0) and at the nozzle exit to resolve boundary layer and rapid expansion of the flow. The far-field boundary is located about five widths of the mixing duct from the shroud so that wall effects may be negligible. In all calculations, a freestream Mach number of 0.2 is used to simulate takeoff conditions and the flow angle at the upstream end is v/u = 0.

Figure 3 shows results for AR's ranging from 1 to 6. Varying the area ratio was accomplished by moving the shroud wall vertically relative to the centerline. Figure 3 shows Mach numbers and pressure contours for the different area ratios at a nozzle stagnation pressure of 3.5 atm and an ambient stagnation pressure of 1 atm, which corresponds to an NPR of 3.5. The nozzle stagnation temperature is 505 K, and the ambient stagnation temperature is 300 K. In all calculations, the Reynolds, Prandtl, and turbulent Prandtl numbers used are 1.3×10^7, 0.72, and 0.9, respectively. The Reynolds number is based on the nozzle width and nozzle exit velocity which would be obtained for an isentropic expansion.

For all area ratios, the Mach number and pressure contours inside the primary nozzle remain unchanged due to the choking at the exit. For the present calculations, the nozzle pressure ratio exceeds the critical pressure ratio (1.9); thus, the flow beyond the nozzle exit becomes supersonic and results in the formation of a series of shock cells. In the present case, the jet boundary is that of a constant pressure and the waves reflected on this boundary become waves of the opposite senses (compression waves are reflected as expansion waves). This mechanism forms a shock cell structure in the underexpanded flow. At AR = 6, the primary flow expands rapidly at the nozzle exit and becomes a jet with a series of shock cell structures. At the secondary flow passage, however, the Mach number is nearly uniform inside the mixing duct. This suggests that freestream flow is passing directly through the mixing duct; hence, mixing between the primary and secondary flows is quite small. The pressure contour also shows nearly uniform pressure through the secondary flow passage. This again indicates uniform flow is passing through without giving efficient pumping.

The results at AR = 2.5 are similar to those at AR = 6. The Mach number contours in the mixing duct still show the uniform flow region, but the incoming flow is more accelerated due to the effective reduction in the secondary flow area between the shroud wall and the jet boundary. Consequently, the rate of mixing increases. The pressure contour also shows an enlarged low pressure region in the mixing duct inlet region, suggesting more effective pumping.

At AR = 1.5, the Mach number changes continuously inside the mixing duct with much faster incoming flow at the mixing duct inlet. Also, the pressure contours show that the mixing duct inlet region is dominated by low pressure,

which leads to more efficient pumping. However, there is a small separation
bubble at the trailing edge region which may deteriorate the thrust perform-
ance. This separation occurs because of a very strong adverse pressure gradi-
ent (shown later in Fig. 5).

The Mach number contour at AR = 1 shows that the jet boundary nearly
impinges on the shroud wall. This behavior reduces the effective secondary
flow area much less than previous cases and the Mach number increases abruptly.
However, Fig. 5 shows that the Mach number at the mixing duct inlet is smaller
than that when AR = 1.5. This suggests that the pumping effect is also
smaller for AR = 1 than it is for AR = 1.5. The reason may be that the jet
boundary, which is hitting the shroud wall, blocks the incoming flow. Also,
the shock cell structure is significantly more distorted than those at larger
area ratios. Unlike the previous cases, the jet boundary is no longer at a
constant pressure, and the pressure varies continuously inside the mixing duct
as shown in Fig. 3. This causes a significant change in the shock cell struc-
ture. Pressure contours also show that pressure at the mixing duct inlet is
higher at AR = 1 than it is at AR = 1.5, which again suggests less effective
pumping at AR = 1.

Some representative streamwise velocity profiles for these cases are shown
in Fig. 4. For the four area ratio cases, velocity profiles are presented at
the three different axial locations noted in Fig. 1. The profile at station 1
is at the exit of the convergent nozzle, and the profiles of stations 2 and 3
are inside the mixing duct region. The streamwise velocity profiles, again,
demonstrate the relatively slow rate of mixing between the primary and second-
ary flows at high area ratios and the increasingly rapid development of flow at
the low area ratios. When the velocity magnitudes at the mixing duct inlet
section are compared, the average velocity at AR = 1.5 is higher than those
velocities at other area ratios. These findings indicate that AR = 1.5 is at
the optimum shroud position for the pumping capability at this NPR.

The calculated shroud surface pressure distribution is shown in Fig. 5.
Cases for four different area ratios have been presented. At AR = 6 and 2.5,
the pressure decreases with downstream distance to reach the minimum near the
inlet section of mixing duct; this causes the secondary flow to accelerate in
the inlet region. The surface pressure then increases as the flow proceeds
downstream until it reaches ambient pressure at the ejector outlet. At
AR = 1.5, the pressure distribution along the shroud wall is quite different
from that for other area ratios. A large pressure dip is found at about
30-percent chord length of the shroud after a smooth pressure decrease in the
inlet region. At these conditions, the interaction between the shock cell
structure of the jet and the shroud wall predominates, which further reduces
the secondary flow passage. The pressure dip is attributed to the previous
interaction phenomena. At AR = 1, the pressure dip is remarkable. The jet
is nearly hitting the shroud wall (refer to Fig. 3). This very strong interac-
tion between the jet and the shroud wall greatly decreases the secondary flow
passage. Flow acceleration through this passage causes the pressure to drop
very quickly (near to the sonic condition). Also, the pressure in the mixing
duct inlet is higher than it is for the AR = 2.5 and 1.5 cases, suggesting a
poor pumping characteristic. The pressure distribution along the airfoil
shroud wall is compared with the experimental data obtained in the NASA Lewis
9 by 15 foot low-speed wind tunnel at corresponding area and nozzle pressure
ratios (Fig. 5). The agreement is quite good at AR = 2.5 over most of the
shroud wall.

A similar set of calculations is shown in Fig. 6 for the case where the nozzle pressure ratio is varied at a constant area ratio. Four nozzle pressure ratio cases have been computed for NPR = 1.5, 2.5, 3.5 and 4.5. Corresponding nozzle stagnation pressures are 1.5, 2.5, 3.5 and 4.5 atm, while the ambient stagnation pressure is kept as 1 atm. In all calculations, AR = 2.5 is used.

Comparing Mach number contours at various pressure ratios shows that as the nozzle pressure increases the shock cell structure becomes larger. At NPR = 1.5, the shock cell structure does not appear because this pressure ratio is below the critical pressure and the jet is entirely subsonic. At NPR = 2.5, the shock cell begins to show up in the vicinity of the nozzle exit; at higher pressure ratios, 3.5 and 4.5, the shock cell becomes larger and propagates further into the downstream region. As mentioned before, this large shock cell structure causes a reduction in the secondary flow area between the shroud wall and the jet boundary and, therefore, the incoming flow into the mixing duct accelerates as the pressure ratio increases. This suggests more efficient pumping at higher pressure ratios. Also, the jet spreading rate increases as the pressure ratio increases.

Pressure contours are also shown in Fig. 6. The development of a shock cell structure can be seen more clearly in these pressure contours. At NPR = 1.5, pressure is nearly uniform inside the mixing duct region without any shock cell. But as the pressure ratio increases, the shock cell becomes larger and stronger. In general, as the pressure ratio increases, the pressure at the mixing duct inlet region decreases. This condition leads to more efficient pumping at higher pressure ratios.

The corresponding pressure distribution on the shroud surface is shown in Fig. 7. In general, the pressure at the mixing duct inlet region decreases as the nozzle pressure ratio increases. As mentioned before, this indicates more pumping at higher pressure ratios. At NPR = 4.5, however, we see a similar behavior to what was seen at AR = 1.5 in Fig. 5. The pressure is at a minimum at around 30 percent of shroud chord length. This occurs because at a high pressure ratio the strong shock cell structure decreases the secondary flow passage and hence the flow accelerates.

The pumping characteristic is an important design parameter of the ejector nozzle for jet noise reduction as well as for ejector performance. Figure 8 shows the pumping characteristic of the ejector nozzle system for various area ratios and nozzle pressure ratios. Computations were made for AR's between 1 and 12 and for NPR's of 2.5, 3.5 and 4.5. The pumping characteristic is expressed in terms of entrained mass flow per unit area (Ws/As). This parameter is a better indicator of pumping than the secondary to primary mass flow ratio (Ws/Wp) when freestream is present. The pumping characteristic is quite low and approaches a certain asymptotic value at high area ratios. This is because at high area ratios the pumping is negligible and most of the mass flow in the secondary passage is due to freestream flow. But as the area ratio decreases, pumping increases and reaches a peak value, depending on nozzle pressure ratio. (At NPR = 3.5 the peak pumping rate occurs at about AR = 1.5; at NPR = 4.5 the peak pumping rate occurs at about AR = 2.5; and at NPR = 2.5, the pumping rate increases until AR = 1 is reached.) A poor pumping characteristic is seen for very low area ratios at NPR = 3.5 and 4.5 because of the blocking effect caused by the shroud wall and the shock cell

structure interaction. It is also anticipated that there is a certain area
ratio for NPR = 2.5 where pumping will be reduced.

Summary

A computational study of the flowfield in a two-dimensional ejector nozzle
has been described. The flow feature inside the ejector nozzle system is com-
plicated by strong inviscid/viscous interaction, freestream entrainment, shock
cell structure, and the presence of both supersonic and subsonic flow regions.
A time-iterative full Navier-Stokes code, PARC, is used to capture this complex
phenomena. A parametric study was made for two controlling parameters, duct to
nozzle area ratio and nozzle pressure ratio. Results show that there is an
optimum area ratio for the efficient pumping of secondary flow. At high area
ratios, the freestream flow passes directly through the mixing duct without
providing adequate pumping. At low area ratios, the jet boundary blocks incom-
ing flow. The nozzle pressure ratio variation shows that the pumping rate
increases as the pressure ratio increases - provided there is no interaction
between the shroud wall and the shock cell structure (i.e., for a certain area
ratio). The comparison with experimental data shows quite good agreement.

Acknowledgment

References

1. Seiner, J.M.; and Krejsa, E.A.: Supersonic Jet Noise and the High Speed
   Civil Transport. AIAA Paper 89-2358, July 1989.

2. Presz, W.M., Jr.; Morin, B.L.; and Gousy, R.G.: Forced Mixer Lobes in
   Ejector Designs. J. Propulsion Power, vol. 4, no. 4, July-Aug. 1988,
   pp. 350-355.

3. Presz, W.M., Jr.; Blinn, R.F.; and Morin, B.L.: Short Efficient Ejector
   Systems. AIAA Paper 87-1837, June 1987.

4. Tillrnan, T.G.; Paterson, R.W.; and Presz, W.M., Jr.: Supersonic Nozzle
   Mixer Ejector. AIAA Paper 89-2925, July 1989.

5. Von Karman, T.: Theoretical Remarks on Thrust Augmentation. Riessner
   Anniversary Volume: Contributions to Applied Mechanics, J.W. Edwards, ed.,
   University of Michigan Press, Ann Arbor, 1949, pp. 461-468.

6. Porter, J.L.; Squyers, R.A.; and Nagaraja, K.S.: An Overview of Ejector
   Theory. AIAA Paper 81-1678, Aug. 1981.

7. Deese, J.E.; and Agarwal, R.K.H.: A Numerical Study of Viscous Flow in
   Inlets and Augmentors. AIAA Paper 88-0187, Jan. 1988.

8. Baldwin, B.S.; and Lomax, H.: Thin Layer Approximation and Algebraic Model for Separated Turbulent Flows. AIAA Paper 78-257, Jan. 1978.

9. Thomas, P.D.: Numerical Method for Predicting Flow Characteristics and Performance of Nonaxisymmetric Nozzles, Theory. NASA CR-3147, 1979.

10. Pulliam, T.H.; and Steger, J.L.: Implicit Finite-Difference Simulations of Three-Dimensional Compressible Flow. AIAA J., vol. 18, no. 2, Feb. 1980, pp. 159-167.

11. Cooper, G.K.: The PARC Code: Theory and Usage. AEDC-TR-87-24, Arnold Engineering Development Center, Arnold AFB, TN, 1987.

12. Douglas, J.; and Gunn, J.E.: A General Formulation of Alternating Direction Method – Part I. Parabolic and Hyperbolic Problems. Numerische Mathematik, vol. 6, 1964, pp. 428-453.

13. Jameson, A.; Schmidt, W.; and Turkel, E.: Numerical Solutions of the Euler Equations by Finite Volume Methods Using Runge-Kutta Time-Stepping Schemes. AIAA Paper 81-1259, 1981.
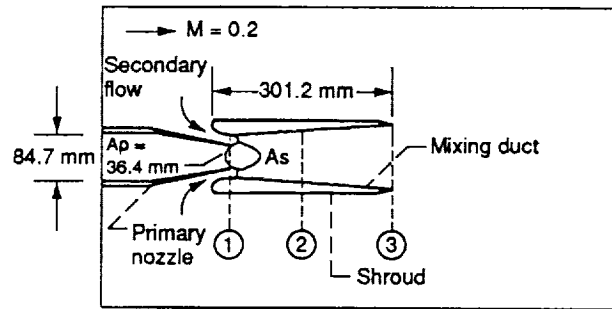
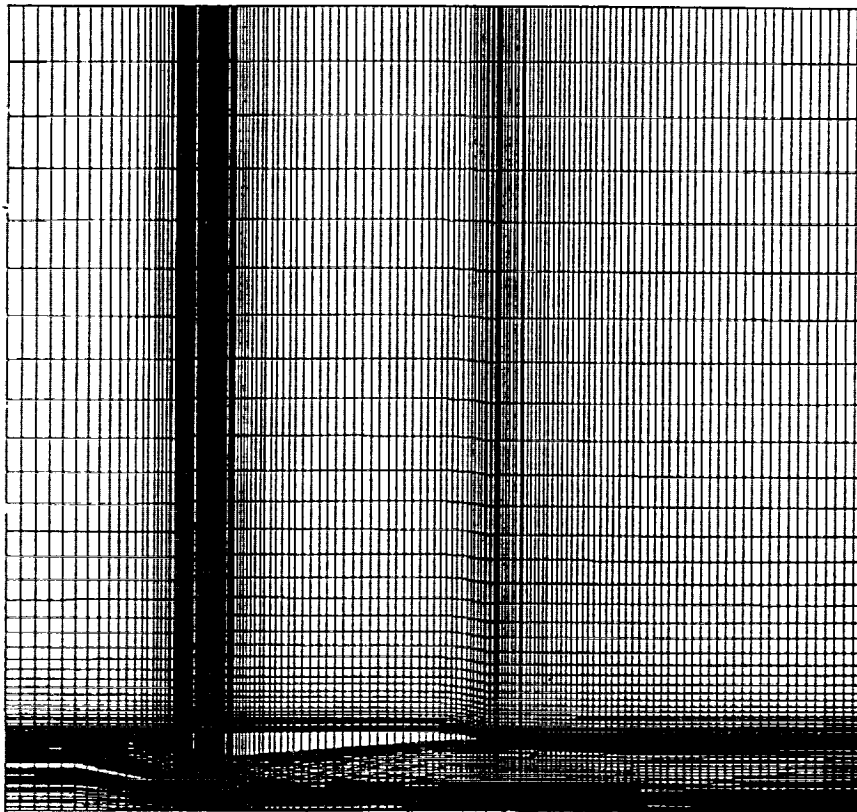Fig. 1. Schematic of two-dimensional ejector nozzle.

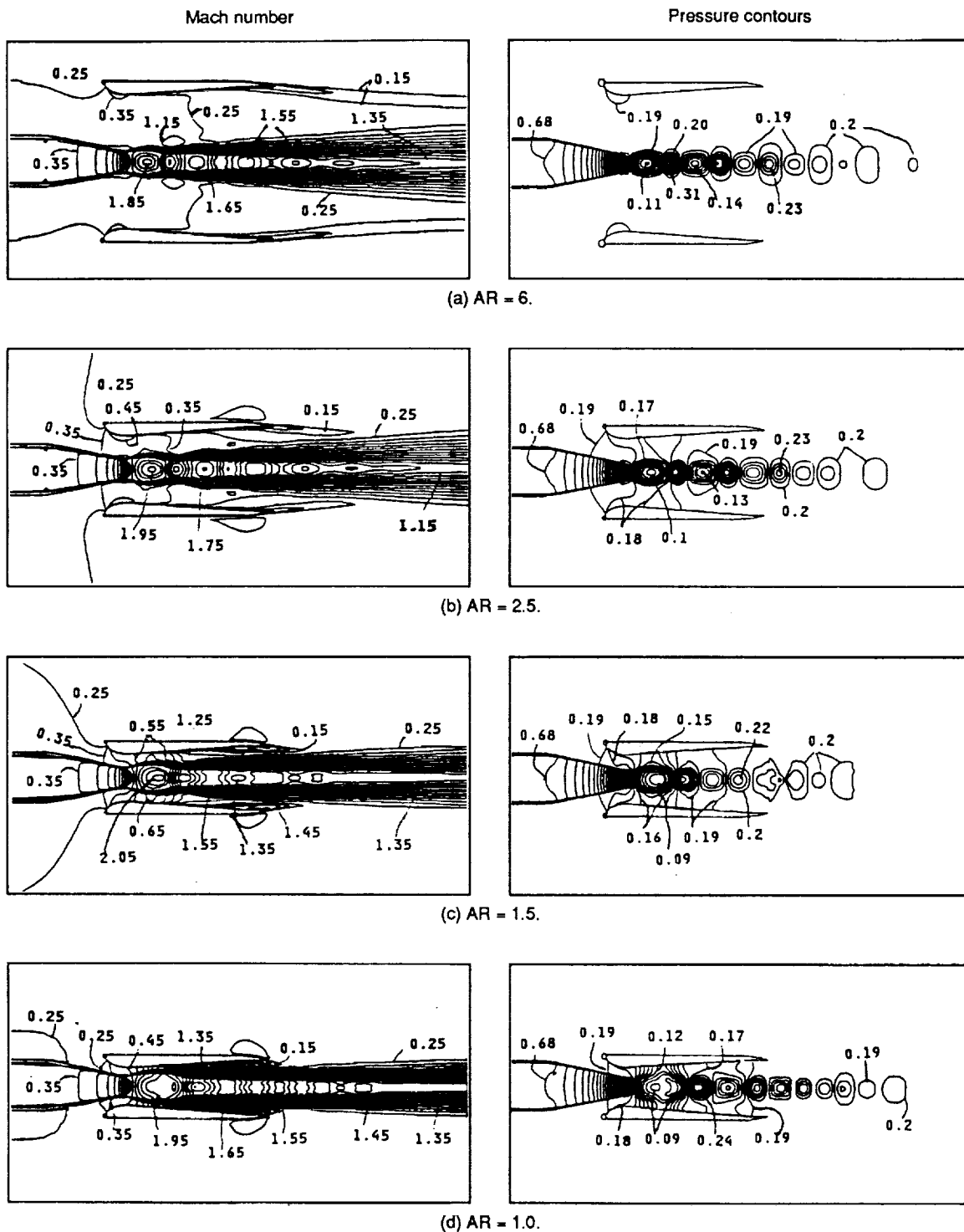Fig. 2. Computational grid for ejector nozzle (171 x 91).

Mach number

Pressure contours

(a) AR = 6.

(b) AR = 2.5.

(c) AR = 1.5.

(d) AR = 1.0.

Fig. 3. Mach number and pressure contours for area ratios (AR) of 6, 2.5, 1.5, and 1 at a nozzle pressure ratio of 3.5.
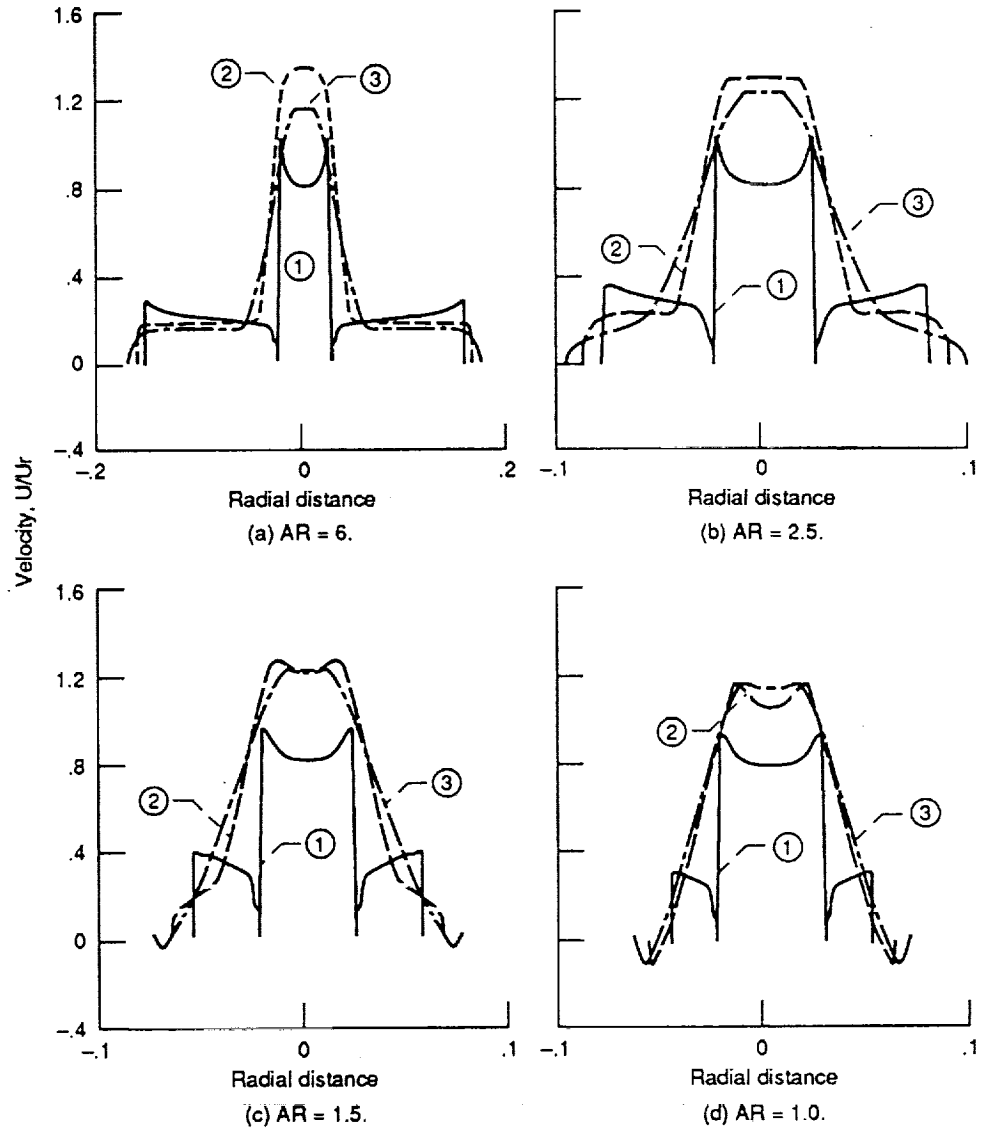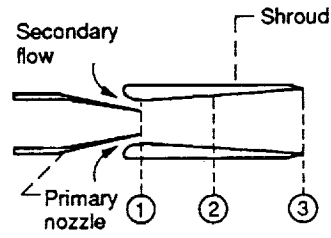
11

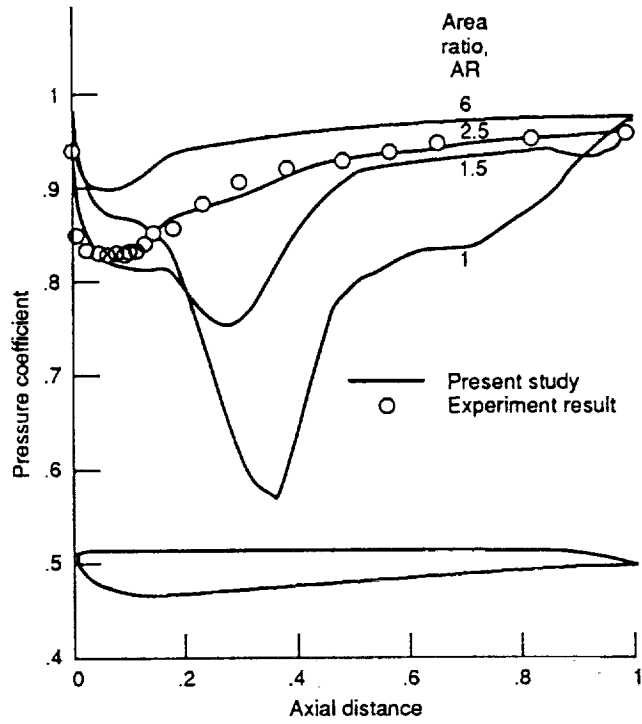Fig. 4. Streamwise velocity profiles for various axial locations and area ratios (AR).

Fig. 5. Pressure distribution on shroud surface.

Mach number

Pressure contours

0.35   0.2
0.3
0.8
0.25   0.7

0.195   0.19
0.29   0.195

(a) NPR = 1.5.

0.25
0.15   0.25
0.35
0.35
0.55
1.15
1.45

0.19   0.18   0.2
0.19
0.48   0.17   0.2
0.18   0.23
0.15

(b) NPR = 2.5.

0.25
0.45   1.15
0.35   0.15   0.25
0.35
1.95   0.35   1.15
1.75

0.19   0.17
0.68   0.19   0.23   0.2
0.13   0.20
0.18

(c) NPR = 3.5.

2.35   1.95   0.15   0.25
0.35
0.35
0.45   1.15   1.45

0.19   0.18   0.19   0.26
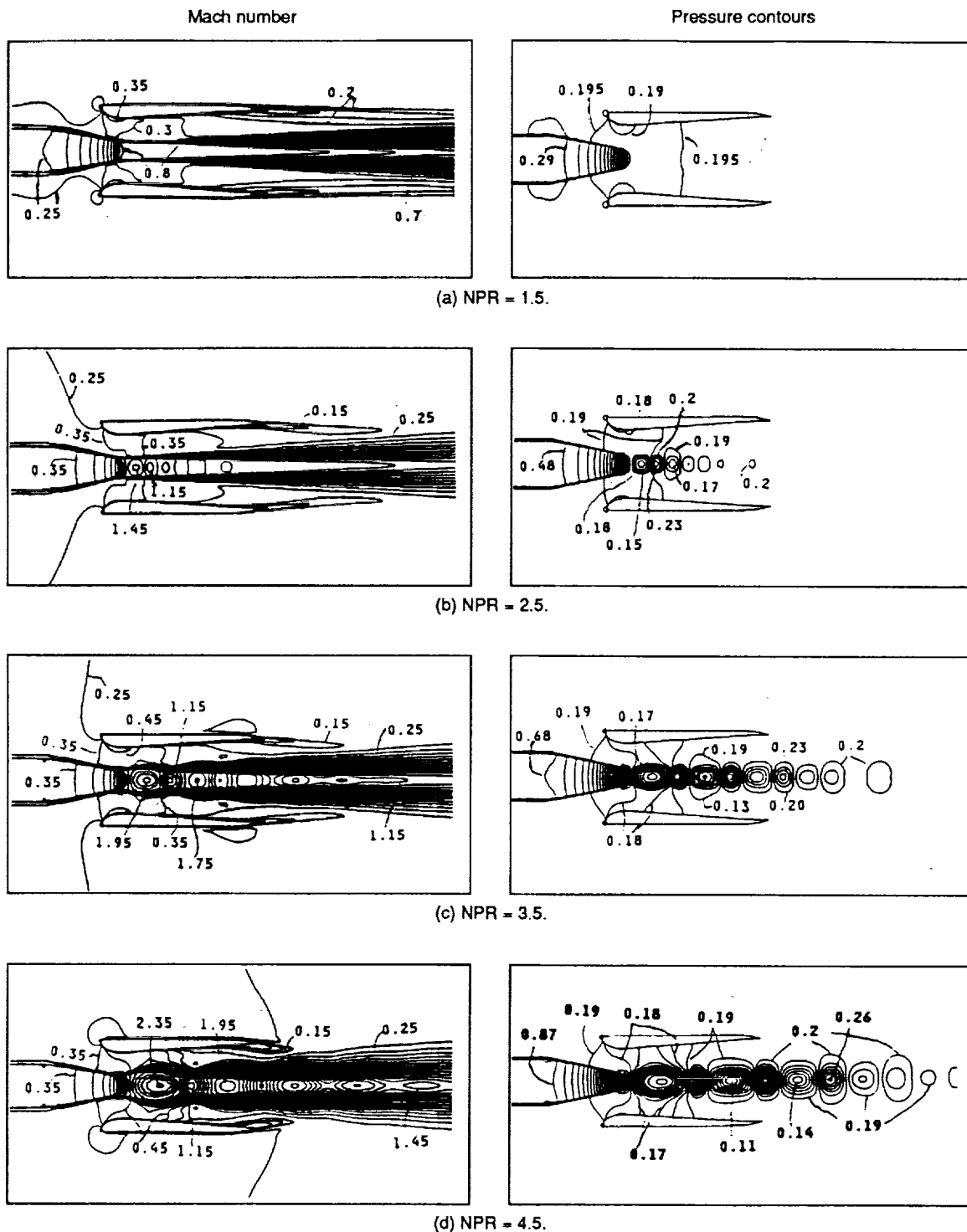0.87   0.2
0.17   0.11   0.14   0.19

(d) NPR = 4.5.

Fig. 6. Mach number and pressure contours for nozzle pressure ratios (NPR) of 1.5, 2.5, 3.5, and 4.5 at an area ratio of 2.5.
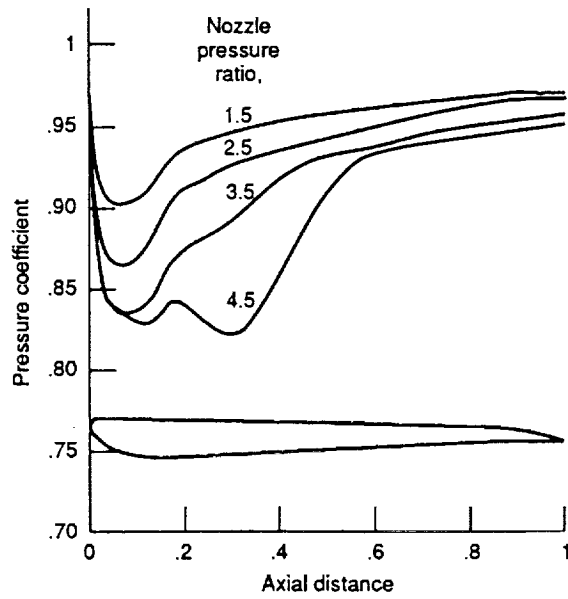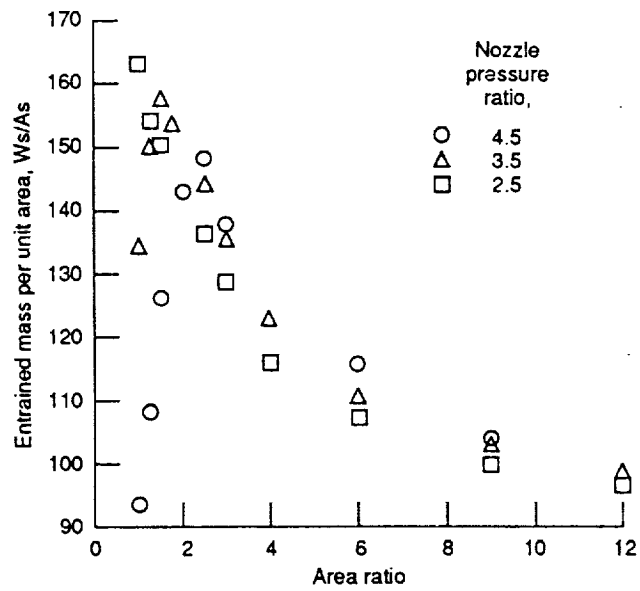
14

Fig. 7. Pressure distribution on the shroud surface.

Fig. 8. Pumping characteristics of ejector nozzle at
various area and nozzle pressure ratios.

Report Documentation Page

1. Report No. NASA CR-185255 AIAA-90-1901	2. Government Accession No.	3. Recipient's Catalog No.

4. Title and Subtitle

Computational Analysis of the Flowfield of a Two-Dimensional Ejector Nozzle

5. Report Date

6. Performing Organization Code

7. Author(s)

Y.H. Choi and W.Y. Soh

8. Performing Organization Report No.

None   (E-5548)

10. Work Unit No.

537-02-41

9. Performing Organization Name and Address

Sverdrup Technology, Inc.
Lewis Research Center Group
2001 Aerospace Parkway
Brook Park, Ohio 44142

11. Contract or Grant No.

NAS3-25266

13. Type of Report and Period Covered

Contractor Report
Final

12. Sponsoring Agency Name and Address

National Aeronautics and Space Administration
Lewis Research Center
Cleveland, Ohio 44135-3191

14. Sponsoring Agency Code

15. Supplementary Notes

16. Abstract

A time-iterative full Navier-Stokes code, PARC, is used to analyze the flowfield of a two-dimensional ejector nozzle system. A parametric study was performed for two controlling parameters, duct to nozzle area ratio and nozzle pressure ratio. Results show that there is an optimum area ratio for the efficient pumping of secondary flow. At high area ratios, a freestream flow passes directly through the mixing duct without giving adequate pumping. At low area ratios, the jet boundary blocks the incoming flow. The nozzle pressure ratio variation shows that the pumping rate increases as the pressure ratio increases, provided there is no interaction between the shroud wall and the shock cell structure.

17. Key Words (Suggested by Author(s))

Ejector flowfield computation

18. Distribution Statement

Unclassified – Unlimited
Subject Category 07

19. Security Classif. (of this report)	20. Security Classif. (of this page)	21. No. of pages	22. Price*
Unclassified	Unclassified	16	A03